



# HHS Public Access

## Author manuscript

*Sci Transl Med.* Author manuscript; available in PMC 2020 February 07.

Author Manuscript

Author Manuscript

Author Manuscript

Author Manuscript

Published in final edited form as:

*Sci Transl Med.* 2019 August 07; 11(504): . doi:10.1126/scitranslmed.aav3505.

## Intranasal micro-optical coherence tomography imaging for cystic fibrosis studies

Hui Min Leung<sup>1,2</sup>, Susan E. Birket<sup>3,4</sup>, Chulho Hyun<sup>1</sup>, Timothy N. Ford<sup>1</sup>, Dongyao Cui<sup>5</sup>, George M. Solomon<sup>3,4</sup>, Ren-Jay Shei<sup>3,4</sup>, Adegboyega Timothy Adewale<sup>3</sup>, Andrew R. Lenzie<sup>3,4</sup>, Courtney M. Fernandez-Petty<sup>3,4</sup>, Hui Zheng<sup>2,6</sup>, Justin H. Palermo<sup>1</sup>, Do-Yeon Cho<sup>3,4</sup>, Bradford A. Woodworth<sup>3,4</sup>, Lael M. Yonker<sup>7</sup>, Bryan P. Hurley<sup>7</sup>, Steven M. Rowe<sup>3,4,\*</sup>, Guillermo J. Tearney<sup>1,2,8,\*</sup>

<sup>1</sup>The Wellman Center for Photomedicine, Massachusetts General Hospital, Boston, MA 02114, USA.

<sup>2</sup>Harvard Medical School, Boston, MA 02114, USA.

<sup>3</sup>Gregory Fleming James Cystic Fibrosis Research Center (Birmingham, AL 35294, USA).

<sup>4</sup>The Department of Medicine, University of Alabama at Birmingham (Birmingham, AL 35294, USA).

<sup>5</sup>Nanyang Technological University (Singapore 639798).

<sup>6</sup>Biostatistics Center, Massachusetts General Hospital (Boston, MA 02114, USA).

<sup>7</sup>Mucosal Immunology and Biology Research Center, Massachusetts General Hospital (Boston, MA 02114, USA).

<sup>8</sup>Department of Pathology, Massachusetts General Hospital, Boston, MA 02114, USA.

### Abstract

Cystic fibrosis (CF) is a genetic disease caused by mutations in the cystic fibrosis transmembrane conductance regulator (CFTR) gene. Although impairment of mucociliary clearance contributes to severe morbidity and mortality in people with CF, a clear understanding of the pathophysiology is lacking. This is in part due to the absence of clinical imaging techniques capable of capturing CFTR-dependent functional metrics at the cellular level. Here, we report the clinical translation of

\*Corresponding author. gtearney@partners.org (G.J.T.), srowe@peds.uab.edu (S.M.R.).

**Author Contributions:** H.M.L., S.E.B., A.T.A., A.R.L., C.M.F.-P., and J.H.P. performed data analysis. H.M.L., C.H., T.N.F., D.C., D.-Y.C., B.A.W., S.M.R., and G.J.T. designed the imaging system. H.M.L., C.H., T.N.F., D.C. built and tested the imaging system. H.M.L., S.E.B., G.M.S., R.-J.S., and S.M.R. acquired clinical data. H.M.L., S.E.B., A.T.A., A.R.L., C.M.F.-P., L.M.Y., B.P.H., and S.M.R., designed and carried out the benchtop experiments. H.Z. supervised the statistical analysis. H.M.L., S.M.R., and G.J.T. wrote the manuscript. S.M.R. and G.J.T. supervised the project, designed the experiments and edited the manuscript. All authors revised and approved the manuscript. G.J.T. and S.M.R. contributed equally as senior authors.

**Competing interests:** GJT and SMR have an unlicensed patent application (US20150253240A1) on the use of μOCT as a diagnostic technology in CF. GJT and DC have an unlicensed patent application (MGH 23814, US Application #15/894,574) on the μOCT probe. G.J.T. is an inventor on patents 14/240,938, 12826303.5, 8896838, 8804126, 5819864, 6029983, 9642531 that cover μOCT imaging. S.M.R. is an inventor on patent 14/240,938 that covers μOCT imaging.

Data and materials availability:

The code that is used for this study is available from the corresponding authors upon reasonable request through a material transfer agreement. All data associated with this study are present in the paper or the Supplementary Materials.

Overline: CYSTIC FIBROSIS

a 1- $\mu$ m resolution micro-optical coherence tomography ( $\mu$ OCT) technology to quantitatively characterize the functional microanatomy of human upper airways. Using a minimally-invasive intranasal imaging approach, we performed a clinical study on age- and sex-matched CF and control groups. We observed delayed mucociliary transport rate at the cellular level, depletion of periciliary liquid layer, and prevalent loss of ciliation in subjects with CF. Distinctive morphological differences in mucus and various forms of epithelial injury were also revealed by  $\mu$ OCT imaging and had prominent effects on the mucociliary transport apparatus. Elevated mucus reflectance intensity in CF, a proxy for viscosity *in situ*, had a dominant effect. These results demonstrate the utility of  $\mu$ OCT to determine epithelial function and monitor disease status of CF airways on a per-patient basis, with applicability for other diseases of mucus clearance.

### One Sentence Summary:

Micro-optical coherence tomography with an intranasal imaging probe detects defects in the mucociliary transport of people with cystic fibrosis.

## Introduction

Cystic fibrosis (CF) is a genetic disease caused by mutations in the CF transmembrane conductance regulator (CFTR) gene. Dysfunctional or absent CFTR function leads to dysregulated epithelial ion transport, adversely impacting multiple organs. The respiratory system is often the most severely impacted, and progressive loss of lung function is the leading cause of CF mortality (1–3). In CF, airway dehydration and abnormally viscous and adhesive mucus are thought to cause a profound decrease in mucus transport, precipitating airway obstruction, chronic infection, and dysregulated inflammation.

Many of our insights regarding CF pathogenesis have been gleaned from animal models and cell culture, generating considerable uncertainty about the mechanisms of human disease. This gap exists because mucus transport abnormalities in CF have been difficult to document in patients (4, 5), particularly at the cellular level. Although useful for monitoring CFTR activity, neither chloride in sweat nor nasal potential difference provide an assessment of underlying pathophysiology of the airway disease (6). Mucociliary clearance (MCC) rate measured by  $\gamma$ -scintigraphy has been a useful assay to estimate within-subject changes in response to interventions, however differences between healthy subjects and those with CF have not always been robust, because increasing central deposition of the radiotracer acts as a covariate that has hampered measurement in patients with airway obstruction (4). Thus, the cardinal pulmonary manifestation of CF, delayed MCC, remains largely presumed in humans, or based on response to CFTR-directed therapeutics (7). Moreover, whether airway dehydration remains a principle component underlying delayed MCC in people with CF, versus driven by inherent abnormalities of mucus, or both, remains subject to intense scientific debate (8–11). Greater knowledge of these mechanisms in patients is necessary to improve disease- and patient-specific interventions. Also, because CF lung disease serves as an important model of other diseases affected by abnormal mucus (such as chronic bronchitis, chronic obstructive pulmonary disease, and asthma), an improved understanding of human CF pathogenesis has broader implications (12).

A clinical tool that can accurately and efficiently capturing key CFTR-dependent functional metrics is therefore highly desirable. Airway optical coherence tomography (OCT), an imaging technique that acquires cross-sectional images of tissue reflectance, has been proposed to address this need (13), but its 10- $\mu\text{m}$  resolution prohibits direct visualization of key microscopic features (cilia, periciliary layer), the function of which are essential to fully characterizing MCC. Other more advanced variations of OCT have also been proposed to study cilia beat frequency (CBF) (14, 15) or mucus flow (16).

Here, we describe the use of a 1- $\mu\text{m}$  resolution form of OCT called micro-OCT ( $\mu\text{OCT}$ ) (12, 17) to extract functional image-based metrics relevant to MCC and CF pathogenesis in the nasal airway (17–20). The nose accurately represents the ion transport environment of the CF airway including genotype-phenotype correlations and the nasal passages remain subject to substantial airway inflammation, providing a window into CF pathobiology (6, 21, 22). We compare nasal  $\mu\text{OCT}$  imaging results from living healthy subjects and subjects with CF. Findings revealed changes in the native microenvironment of CF airways, providing a physiologically-intact framework for studying important aspects of CF airway disease pathogenesis in humans.

## Results

### Imaging procedure and subjects

For human airway  $\mu\text{OCT}$  imaging, a fiber-optic catheter that implements the benchtop optical interferometric design was developed. We previously reported the use of a 4 mm rigid custom-built  $\mu\text{OCT}$  imaging catheter to perform swine trachea imaging *in vivo* (23). Subsequently, a semi-flexible 2.4 mm diameter side-viewing  $\mu\text{OCT}$  imaging catheter was developed to facilitate navigation in the airways (24). Based on the latter design, a transportable clinical-grade intranasal  $\mu\text{OCT}$  imaging catheter and console (Methods and Materials section:  *$\mu\text{OCT}$  technology*) were developed to study the upper airways of human subjects (Fig. 1A). Each study participant was imaged unsedated in a standard clinical examination room with the participant's head on an ophthalmologic head brace. After nasal inspection with an illuminating rhinoscope, the clinician maneuvered the  $\mu\text{OCT}$  probe into the subject's nasal inferior meatus region while visualizing  $\mu\text{OCT}$  images in real time (Fig. 1B and C). With the probe held steady, 30-second  $\mu\text{OCT}$  videos were acquired from approximately five discrete sites at each anatomical region (turbinate and floor) of each naris. Insertion of the probe was gentle and non-traumatic. A total of 20 subjects (CF  $n = 10$ ; non-CF  $n = 10$ ) were enrolled and all subjects completed the procedure successfully with minimal discomfort. No mucosal swelling or injury was observed during or immediately after the procedures. Participant demographics and clinical characteristics are shown in table S1. There were no statistical differences in sex, age, and race of the study participants between the CF and non-CF groups. All subjects with CF harbored severe, non-functional CFTR mutations. The mean duration of each imaging session was 25 minutes [CF 24(6) minutes; non-CF 26(11) minutes]. Of the 20 subjects imaged, the success rate of making at least three technical replicates of each of the quantitative metrics per subject ranged from 70–100%. Intra- and inter-observer agreements were high for all measurements, exceeding 0.98 and 0.88, respectively, for each metric (Table 1). There were no clinically meaningful

adverse complications associated with the imaging procedure, and there were no issues with subject tolerance. One healthy volunteer had transient mild epistaxis 24 hours after the procedure that resolved without specific intervention.

### Diminished PCL, CBF, and MCT in subjects with CF

Scatter plots depicting measurements of the five metrics used to assess the functional nasal airway microanatomy are shown in Fig. 2A to E. Periciliary liquid layer depth (PCL,  $P<0.01$ ), mucociliary transport rate (MCT,  $P<0.0001$ ), and ciliary beat frequency (CBF,  $P<0.05$ ) in the CF cohort were significantly lower than those in the non-CF cohort (Fig. 2A to E, Table 1). Representative  $\mu$ OCT images and videos from subjects who are healthy and with CF (Fig. 3A to H and videos S1 and S2, respectively) identified substantial differences between the two cohorts. These results demonstrate PCL depletion, a marker of airway dehydration, and delayed MCT at the cellular level in people with CF *in vivo*. In contrast, no statistical differences between the two cohorts were found for airway surface liquid layer depth (ASL), which incorporates both the PCL and the overlying mucus, or epithelium thickness (ET).

Across all subjects, we observed a positive linear correlation between PCL and MCT (Fig. 2F;  $r = 0.68$ ;  $P<0.01$ ) and CBF versus MCT (Fig. 2G;  $r = 0.56$ ;  $P<0.05$ ), relationships first detected using co-localized  $\mu$ OCT measures in swine trachea (11). In contrast to PCL, a quadratic relation was found between mucus depth measured by ASL and MCT (Fig. 2H;  $R^2 = 0.56$ ;  $P<0.05$ ), with an optimal ASL depth ( $\sim 50 \mu\text{m}$ ) associated with maximal MCT; lower MCT was found with higher ASL thicknesses -- largely in association with CF.

*Disruption of PCL, loss of ciliation, and damaged epithelium observed in subjects with CF*  
Other structural abnormalities were also evident in the epithelium of subjects with CF. In healthy subjects, a continuous dark band between mucus and the epithelium indicated the absence of mucus infiltration into the PCL (11). The integrity of the PCL was intact even when the imaging probe was pushing the mucus against the epithelium (Fig. 3B). Although evidence of similarly intact PCL could also be observed in subjects with CF (Fig. 3C), there were several other heretofore unrecognized abnormalities, including a disrupted PCL seen as gaps between motile cilia (pseudo-colored in green) that was more prevalent among subjects with CF (Fig. 3D to F). This was evident in the significantly lower estimated percent cilia coverage (pCC) on epithelial surfaces of subjects with CF than on healthy subjects (Fig. 3I;  $P<0.05$ ). Our data also showed a positive correlation between pCC and MCT (Fig. 3J;  $r = 0.53$ ;  $P<0.05$ ).

The potential impact of cilia disruption on the mucus clearance in CF has not been previously reported. As a seminal example of the implications of this defect, Fig. 3D shows that the PCL underneath a thick mucus layer was compromised, containing gaps in a subject with CF, despite being moderately well-ciliated. The overlying mucus infiltrated the ciliary layer and was in direct contact with the underlying epithelium, suggesting the potential for adhesive events. Fig. 3E depicts a more severe example of a discontinuous PCL due to partial loss of epithelial ciliation. Fig. 3F shows a case where the epithelium was almost completely unciliated, apart from a few isolated regions, including mucus in direct contact with collapsed cilia. No PCL was perceptible and the area with a collapsed PCL was

Author Manuscript  
Author Manuscript  
Author Manuscript  
Author Manuscript

accompanied by a thick mucus layer, quantified as an ASL of more than 50  $\mu\text{m}$  that was in direct contact with the epithelium (Fig. 3F). Fig. 3G shows a case where the epithelium was completely unciliated. Denuded epithelial surfaces (evidence of epithelial injury) were frequently observed (Fig. 3H). Damaged epithelial surfaces were highly uneven and completely devoid of any ciliary activity or identifiable PCL.

### Obstructive airway glands in CF

Concomitant with structural abnormalities in the ciliary layer and epithelial damage, large (~70–100  $\mu\text{m}$ ) round and bright structures were seen in the mucosa of a few subjects with CF (Fig. 4A and B), suggestive of inspissated mucus in obstructed airway glands, as reported in the earliest descriptions of the disease (25), CF piglets (26) and CF rats (27). In contrast, a typical image of an unobstructed healthy gland is shown in Fig. 4C.

### Heterogeneous CF mucus structures

Representative  $\mu\text{OCT}$  images taken from healthy subjects (Fig. 5A to C) were juxtaposed with those from CF subjects (Fig. 5D to F). Common among images from healthy subjects was the presence of a thick and contiguous PCL layer that spanned the epithelial surfaces. Mucus of healthy subjects (indicated by M in Fig. 5A to C) was typically weakly visible with brighter particulates sparsely occupying the layer. Although ASL thicknesses in healthy subjects were highly variable, mucus from healthy subjects generally preserved those same characteristics (Fig. 2D, Fig. 5A to C). In stark contrast, the bulk of the mucus in subjects with CF (indicated as M in Fig. 5D to F) often appeared bright and took on various forms of heterogeneity with structural features within the mucus. Such optically bright and heterogeneous CF mucus sometimes achieved thicknesses greater than 100  $\mu\text{m}$  (Fig. 5D to F), obscuring the view of underlying epithelial tissue.

### CF mucus exhibited higher optical reflectivity

Sputum from CF and healthy subjects were obtained and split into aliquots for separate analysis on a cone-and-plate rheometer and under a benchtop  $\mu\text{OCT}$  system (Supplementary material, Ex vivo sputum analysis). Sputum samples from subjects with CF exhibited increased dynamic viscosity as compared to those from normal individuals that was most prominent at low shear rates (fig. S1B and C). It was also found that  $\mu\text{OCT}$  reflectance intensity was strongly correlated with dynamic viscosity of expectorated sputum (fig. S1F;  $r=0.63$ ,  $P<0.05$ ). Given these results indicating that reflectivity can serve as an indicator of sputum dynamic viscosity and noting the marked differences in the intensity of light scatter in the mucus layer of subjects with CF as compared to healthy individuals (Fig. 5G), we conducted an analysis of reflectance intensity of the mucus layer acquired *in vivo* and analyzed data by diagnosis (fig. S2). A representative  $\mu\text{OCT}$  image of mucus from a healthy subject (fig. S2A) showed presence of small particles and mild reflectance intensity. In contrast, a representative  $\mu\text{OCT}$  image of mucus from a subject with CF (fig. S2B) showed larger particles with stronger backscattering properties. Mean mucus reflectance intensity measurements demonstrated that subjects with CF have more intensely reflective mucus as compared to controls (Fig. 5G,  $P<0.01$ ), indicative of increased viscosity of airway mucus *in situ* and *in vivo*. Mean reflectance intensity of mucus *in vivo* was inversely correlated to

airway hydration, as reflected by PCL depth ( $r = -0.64$ ,  $P < 0.01$ ; Fig. 5H) and MCT rate ( $r = -0.58$ ,  $P < 0.05$ ; Fig. 5I).

### Prevalence of globules in CF mucus

Fig. 6A and B depict other types of epithelial injury observed in images from subjects with CF, where the epithelial surfaces were completely unciliated. In these instances, segregation of bright granulocyte-appearing spherical globules was observed in regions immediately beneath the epithelial surfaces (Fig. 6A and B). Highly light scattering structures of similar sizes and appearance were also observed atop the epithelium (Fig. 6B) and embedded in secreted mucus in different concentrations (Fig. 6C to F). Although the concentrations of granulocyte-appearing globules varied among different subjects (Fig. 6C to F), their sizes and optical characteristics were similar across all subjects that exhibited such features. The mean diameter of these globules was 10.9 (10.39 – 11.41)  $\mu\text{m}$  (Supplementary materials: Image processing methods). The mean number of globules observed per image frame in  $\mu\text{OCT}$  videos of CF mucus was significantly higher than that of the mucus of healthy subjects (non-CF 0.06 (0.01 – 1.11) per frame; CF 1.00 (–0.08 – 2.09) per frame;  $P < 0.01$ ; Fig. 6G). In addition, it was found that pCC decreased as the number of granulocyte-appearing globules increased, as illustrated in the semi-log plot of pCC versus mean frame globule count ( $r = -0.5716$ ;  $P < 0.01$ ; Fig. 6H).

To find out if the globules could be granulocytes, their sizes and optical characteristics were compared with human granulocytes used in an in vitro  $\mu\text{OCT}$  neutrophil trans-epithelial migration experiment similar to those detailed in ref. (28) (briefly described in Granulocytes characterization section of Supplementary material). After breaching the monolayers, the human neutrophils did not immediately detach from the monolayer and, instead, formed columns of neutrophils (indicated as NC in fig. S3A and B). The neutrophils are optically brighter than the cell monolayer and their bead-like appearances, even when aggregated, can be appreciated. An image showing a cell monolayer without addition of neutrophils is shown in fig. S3C for comparison. The average diameter of individual neutrophils (indicated with arrowheads), which started to detach after a certain period of time, was measured to be 9.2 (8.5–10.0)  $\mu\text{m}$ . This result was similar to measurements of the globules in in vivo mucus images. To further find out how neutrophils appear within mucus, we used benchtop  $\mu\text{OCT}$  to image swine mucus mixed with human granulocytes (fig. S4A). A sample of swine mucus with naturally occurring granulocytes was additionally imaged with  $\mu\text{OCT}$  (fig. S4C). The appearance of the bright and round globules in these images (fig. S4A and C) closely resembled what was observed in in vivo images acquired from human subjects. Giemsa-stained smears of both swine mucus samples showing prevalence of multi-lobular neutrophils are given in fig. S4B and D. In both cases, individual granulocytes and neutrophils could be visualized by  $\mu\text{OCT}$  even when embedded within native swine mucus (fig. S4A and C). These results serve to strengthen the point that globules embedded within human mucus as seen with intranasal  $\mu\text{OCT}$  are indeed granulocyte-dominated inflammatory cells.

## Quantitative relationships with MCT

Univariate analysis demonstrated PCL depth (Fig. 2F), CBF (Fig. 2G), functional ciliary expression (pCC, Fig. 3J), and mucus optical reflectance intensity (Fig. 5I) were linearly correlated to MCT (summarized in table S2). To assess their relative effects and determine which factors were independently associated with delayed MCT, we performed stepwise multivariate regression. Findings showed that the starting 5-variable model (CBF, mean intensity of ASL, pCC, PCL, and mean frame globule count) had an  $R^2$  of 0.7526 (model #1 in table S3,  $P<0.05$ ), indicating that  $\mu$ OCT-derived parameters have a substantial capacity to predict MCT. Stepwise multivariate regression resulted in a 2-parameter model that included CBF and ASL intensity ( $R^2=0.6783$ ;  $P<0.01$ ; model #2 in table S3) that was sufficient to determine a large portion of MCT delays. This result suggests that mucus viscosity and CBF are the largest independent contributors to the magnitude of the CF mucus clearance defect. By including the consideration of first-order interaction terms, two 2-parameter models were found to have improved capacity to explain the data (higher  $R^2$  and comparable or better  $P$ -values). The first model included mean intensity of ASL and CBF $\times$ PCL ( $R^2=0.6978$ ;  $P<0.01$ ; model #3 in table S3), whereas the second model included mean intensity of ASL and pCC $\times$ mean intensity of ASL ( $R^2=0.7239$ ;  $P<0.001$ ; model #4 in table S3). Models #2, 3, and 4 each included the mean intensity of ASL as the largest standardized  $\beta$  value, suggesting that mucus viscosity has a dominant effect on modulating MCT. A comparison of model #2 and #3 suggests that although CBF is also critical in determining MCT, the presence of a healthy amount of epithelial hydration may possess important additive effects.

Although our univariate correlation results for the different metrics were statistically significant,  $R^2$  values demonstrated moderate correlations between those metrics and MCT. Thus, there is still some variation that is not explained by these univariate relationships. Nevertheless, in the multivariate regression analyses, statistically significant models with substantially improved  $R^2$  values were derived. This suggests that when all defects in the functional microanatomy are considered, prediction capacity is substantially enhanced compared to measuring individual parameters alone, and that defects have cumulative effects.

## Discussion

Here we used intranasal  $\mu$ OCT imaging as a minimally-invasive means to perform *in vivo* functional microscopic imaging of upper respiratory tracts of human subjects. This technology is unique in that it enables longitudinal clinical studies of function, microanatomy, and dynamic events in human airway with subcellular resolution. The cross-sectional  $\mu$ OCT videos provide imaging data for quantitative subject-specific measurements of important functional microanatomy (PCL, ASL, CBF, MCT, and ET) that are relevant to understanding the pathophysiology underlying impaired MCC and additional qualitative findings that are highly illustrative of airway disease pathogenesis.

The newly developed clinical  $\mu$ OCT system was used to perform a CF clinical study involving 20 subjects with no clinically meaningful adverse complications, and the brevity and safety of the imaging sessions open new possibilities in disease understanding and management. The results from this study indicate that people with CF exhibit depleted PCL,

decreased CBF, and low MCT at the cellular level, supporting a longstanding but controversial hypothesis that dysregulated mucus hydration is a key feature that underlies CF pathogenesis. Through positive correlations between MCT versus CBF and PCL, functional imaging revealed that both ciliary action and epithelial hydration are important factors that promote MCT *in vivo*. The presence of thick layers of highly heterogeneous CF mucus that was both highly reflective (viscous) and with distinctive, highly banded patterns and microstructures indicates that CF mucus is also inherently abnormal and can contribute to mucus stasis itself. Together with evidence of infiltration of inflammatory cells into CF mucus (as observed with  $\mu$ OCT imaging) and its consequences on epithelial homeostasis,  $\mu$ OCT demonstrates the capacity for improving our understanding of a variety of airway disorders in patients. Now that we have shown the microstructural and functional differences between healthy and CF airways, an important next step would be to observe and quantify changes in this functional microanatomy, including MCC, in response to bioactive pharmacologic modulation, particularly those that activate CFTR.

Our findings support the hypothesis that there is a mechanistic breakdown of airway host defense in people with CF where CFTR-dependent processes are dysregulated. Ionic imbalance across the epithelium creates an osmotic pressure that further mediates the depletion of the PCL layer (11, 29). The decrease in water content within CF ASL may be inferred from the diminished PCL depths we found within the CF cohort. A uniform and clear PCL gel has the ability to prevent mucus load from coming in direct contact with the epithelium, allowing ciliary action to take place unencumbered. However, prevalent disruption of the PCL and lower cilia coverage were often observed in subjects with CF. In cases of severe loss of ciliation, we observed a collapse of the PCL that precipitated mucus adhesion to the airway surface, a phenomenon postulated to occur (11) but heretofore not witnessed clinically, and, in part, a plausible explanation for the heterogeneous expression of obstructive airway events in people with CF. Compromised PCL integrity, particularly when coupled with mucus hyperviscosity, makes mucus resistant to locomotive action from beating cilia. Accumulation of resident mucus overburdens the cilia layer and causes the autoregulatory response of stimulated CBF to fail (30). This phenomenon may be exacerbated further by gaps in ciliation. Our data showed that subjects with CF exhibited a significantly lower MCT and CBF than control subjects; prior studies have shown CBF in CF epithelium can be normal when overlying mucus is not involved (18). Positive correlations found between PCL versus MCT and CBF versus MCT in humans *in vivo*, a finding previously observed in excised swine trachea (18), lend further support to the notion that PCL and CBF play important roles in promoting MCC.

Several distinctive features of airway disease that we observed using intranasal  $\mu$ OCT in human subjects had not been readily seen previously using *in vitro* or *ex vivo* models; these findings provide insights into CF pathogenesis related to inherent abnormalities of CF mucus. The differences in the appearances of CF mucus was evident: Non-CF mucus was predominantly hyporeflective with bright and small particles sparsely dispersed within it, whereas CF mucus was often hyperreflective. This implies that CF mucus was concentrated with substances that conferred much stronger backscattering properties, a finding associated with increased viscosity of expectorated sputum. However, CF mucus also had heterogeneous but clearly defined structures within the mucus, indicative of differences of

Author Manuscript  
Author Manuscript  
Author Manuscript  
Author Manuscript

the mucus itself. Mucin composition, the molecular unfolding of mucins, and their oxidation status have all been postulated to be important factors affecting mucus properties and are abnormal in CF (31–35). These factors determine the different types of polymerized networks within mucus that determine its microrheology and transportability across the epithelium. The manner by which layers of mucus form and fold may indicate differences in the mucus polymerization network among people with CF. Similarly, obstructed airway glands were observed in CF samples. In total, these observations are reminiscent of findings in newborn pigs where bands of mucus were observed emanating from CF goblet cells and the outlet of airway glands, which were shown to occur even in submerged conditions, thus ruling out airway dehydration as the sole cause of impaired MCC (26, 31, 36). Regression analysis supported this observation, revealing that mucus reflectance intensity is one of the strongest independent predictors of the MCT abnormality (standardized  $\beta$ ) and also was included in the most parsimonious predictive model, including several alternative analyses.

The current study did not find a significant difference in ASL, principally a measure of mucus layer depth, between CF and non-CF cohorts, driven in part by the fact that subjects with CF accounted for the highest ASL depths measured and this was associated with slower MCT. This might, at first, seem to contradict the hypothesis that CFTR-dependent epithelial hydration was decreased in people with CF, and may have contributed to a previous controversy (8, 26). Nevertheless, the quadratic relation found between ASL and MCT suggests that a positive relationship exists between ASL and MCT up to a point when ASL becomes excessive (approximately above 50  $\mu\text{m}$ ), above which the higher ASL is detrimental to MCT. This observation was noted in a porcine model of CF, which ultimately indicated the presence of inherent abnormalities to the mucus layer prone to mucus accumulation (18). Increased reflectivity of the overlying mucus in people with CF, a proxy for viscosity, supports this reasoning. In the healthy physiologic range of ASL and in the absence of aberrant mucus, greater ASL depths indicate a higher CFTR-dependent hydration. But when excessively thick mucus sets in at greater mucus depths ( $>50 \mu\text{m}$ ), ASL measurements become a reflection of severity of mucostasis due both to loss of water content in the ASL and its inherent hyperviscous characteristics. These data are consistent with similar observations in excised CF and non-CF pig trachea (30). Although previous ex vivo studies (18) observed a negative correlation between ASL and MCT in CFTR<sup>-/-</sup> swine trachea, this relationship was analyzed independent of the control group, in which ASL depth and MCT were positively correlated at low ASL depths (thus accounting for the quadratic relationship observed here when both are combined).

Our results are aligned with a unifying hypothesis that dysregulation of hydration content due to ionic imbalances across epithelial surfaces can serve as the nidus for CF pulmonary morbidity (37), while excess mucus viscosity is a dominant aspect that independently contributes to mucus stasis and likely contributes to mucus adhesion to the epithelial surface (18, 35, 36, 38). Although higher mucus solid content or refractive index could be due to decreased epithelial hydration and/or increased secretion of mucins (11, 29, 39), the structural differences within the mucus itself, and its heterogeneous nature readily apparent by  $\mu\text{OCT}$ , are unlikely to be explained solely by dehydration events; hydration abnormalities alone would be expected to be homogenous in nature due to the free movement of water in the mucus layer, and the nasal environment provides near saturated humidity within the

inferior meatus (40). Confirmatory studies in larger patient groups and in response to the activation of CFTR would provide additional supportive evidence.

Unlike previous work by other groups (41, 42) that reported a difference in ET between subjects with CF and non-CF controls using a lower resolution, conventional form of OCT to image the nasal airways, our results showed no statistically significant difference in ET. It should be noted that there was a discrepancy in measured nasal ET among previous reports using similar techniques. This suggests possible difficulties in precisely determining the boundary between the epithelium and submucosa with conventional OCT. Therefore, we postulate that the absence of a difference in ET observed in our study could be due to higher measurement precision by  $\mu$ OCT, although differences in the severity of CF between the study samples remains possible.

Despite being abundant in mucus, mucins do not solely account for the properties observed in human mucus (43). Other major polymerizing constituents such as actin and by-products of degraded neutrophils have been discovered to play important roles in modulating viscoelastic properties of mucus (43). Our data indicate that CF airways often suffer epithelial injury (denuded epithelium), a heretofore unrecognized pathology that can have an important influence on MCT. Inflammatory cells such as eosinophils and neutrophils are recruited to inflamed sites, and in light of the important role of these cells in both acute and chronic inflammation (44), the effect of inflammation severity on mucus clearance could be considerable. We observed  $\sim 10 \mu\text{m}$  diameter spherical globules segregated at the top regions of an unciliated epithelium, directly on the surface of the unciliated epithelium, and as discrete structures embedded within secreted mucus. The measured diameters of these globules were similar to those of inflammatory cells such as neutrophils (45, 46, 47). In addition, these globules bore close resemblance to neutrophils observed in  $\mu$ OCT images recorded from an *in vitro* transepithelial neutrophil migration experiment. The similarity in optical properties and sizes between these highly reflective globules and neutrophils, and the observation that they transit from unciliated epithelium to mucus, support the notion that these structures represent inflammatory cells. An elevated density of these structures was observed only in the CF cohort, although both subjects with and without CF could exhibit infiltration of globules in mucus.

Because loss of ciliation is likely a sign of acquired epithelial damage, the presumably active inflammatory response we observed in regions of CF images supports epithelial injury at those locations. A positive correlation between cilia coverage on epithelial surfaces and MCT suggests that epithelial injury and loss of cilia can contribute to impairment of MCT. A negative correlation between pCC and mean frame globule count provides further evidence of the deleterious effect of inflammatory response on epithelial damage and, hence, MCT. Based on the observed influx of presumed inflammatory cells in mucus and in the epithelium, these cells and their subsequent degraded forms could affect mucus microrheological properties and its capacity to be expelled from the airways in people with CF. The capability of  $\mu$ OCT to visualize these cells could be useful for characterizing and monitoring inflammation in CF and other epithelial diseases *in vivo*.

A limitation of this intranasal μOCT technology pertains to the stabilization of μOCT image frames for further image analysis. Obviating the sedation of imaged subjects is key to keeping the imaging sessions brief and making it feasible for conducting longitudinal studies on human subjects that require multiple imaging sessions. However, the inevitable presence of relative motion between the subject and the imaging probe during data acquisition necessitated the use of post-processing to stabilize the movies. The 2D cross-correlation technique employed in this study was meant to address motion artifacts that occurred in the cross-sectional plane as defined by the direction of the scanning beam. However, it did not correct for 3D motion artifacts; measurements were thus excluded when 3D motion prohibited the accurate determination of parameters. Constraints that qualify certain image frames for analysis of the various metrics of interest prevented co-localized measurements of all metrics from being made in every instance. In other words, measurements present subject-specific, but not site-specific, results. We expect future enhancement of the imaging system with probe-stabilizing mechanisms (48), which could have the potential to augment the number of colocalized results, allowing region-specific covariates to be determined *in vivo* in the future. This will enable experimental intervention studies and allow confirmation of the findings related to epithelial dysfunction and their relationship to CFTR activity when combined with agents that activate ion transport or interfere with mucus homeostasis.

## Materials and methods

### Study design

The goal of our study was to use μOCT to perform live imaging of human airways with subcellular resolution to understand the pathophysiology of CF. With the use of an intranasal imaging probe, μOCT videos of the upper airways of age- and sex-matched study participants (healthy or having CF) were recorded. Through quantitative analysis of the μOCT videos, a comparative study of various aspects of the airway functional microanatomy between the CF and healthy controls were carried out in an effort to understand CF airway pathophysiologies in clinical settings. The study was approved by The Partners IRB (Protocol # 2016-P000272) and University of Alabama IRB (Protocol # F160125001); [ClinicalTrials.gov](#) Identifier: [NCT03256773](#). For first-in-human use, eligibility criteria for voluntary participation included age between 18 and 70, and no recent respiratory infections requiring antibiotics or corticosteroids 4 weeks prior to the study. CF volunteers had a confirmed diagnosis of cystic fibrosis, were clinically stable without acute respiratory or sinus exacerbation of illness within two weeks of the single-day study visit. Subjects with CF who have a history of prior sinus surgery expected to substantially disrupt the normal anatomy were also excluded. Non-CF controls subjects excluded a history of acute or chronic sinus disease or other chronic respiratory diagnoses. Pregnancy and a history of major sinus surgery that would alter the nasal anatomy were additional exclusions. Non-CF control subjects were recruited to generally age match the CF cohort.

The raw data which contained the μOCT spectrograms were recorded locally and automatically duplicated onto a separate local drive upon completion of each imaging session. The data was regularly transferred to an off-site server and a copy was directly

transferred to an image analyst without further blinding for image analysis, according to methods described in the Image processing section.

Due to absence of earlier similar human studies, the calculation of cohort size was estimated based on previous ex vivo swine studies (18), assuming a statistical power of 80% and a two-tailed *t*-test. Measurements from each different imaged nasal region were treated as independent technical replicates to obtain the mean values of the different metrics for each subject. At least three valid measurements for each metric per subject was necessary to include that metric in subsequent cohort and regression analyses. Intra- and inter-observer reliability measurements were performed by two independent observers on a randomized subset (approximately 10%) of the data. Intra-observer reliability was tested after a 20-week washout period (table 1 and fig. S5.). One of the observers completed the measurements on the remainder of the data. The data files were serially named by the order which they were acquired, by unique subject ID numbers and time stamps. There was no further de-identification or blinding of the data files.

### **μOCT technology**

The μOCT technology has been described in previous publications (12, 23) and is shown in Fig. 1. In brief, the device is based on the principles of spectrometer-based spectral-domain OCT. Broadband light from a supercontinuum laser (SuperK Extreme OCT, NKT Photonics) was first filtered to achieve a Gaussian-like spectral shape. A beam splitter then directed a portion of the light to a custom-built, common-path interferometer, intranasal μOCT catheter that focused a hybrid annular imaging beam and directed it to the side. The use of the annular imaging beam created a Gaussian-Bessel intensity distribution at the focus, allowing high lateral resolution over an extended depth of focus (12). Through linear motion transduced by a piezoelectric motor (Physik Instrumente), housed within an electrically isolated handle unit, the beam was scanned longitudinally over a distance of 350 μm at a rate of 40 Hz. This rapid scanning action occurred within a sterile, single-use sheath that was fitted over the fiber-optic core and fixed onto the handle unit. Each sheath had a transparent window at the distal end to allow transmission of the optical beam. The assembled unit had a catheter length of 15 cm and outer diameter of 2.4 mm. Light returning from the tissue was relayed to a spectrometer constructed from a 940 linepairs/mm volume phase holographic grating (Wasatch Photonics), a camera lens (Nikon) and a CMOS line scan camera (spL4096–140km, Basler AG). The spectrometer detected a full-width-half-maximum spectral range of  $800 \pm 150$  nm and 2500-pixel spectrograms were recorded at a rate of 20 kHz during data acquisition. Spectra were remapped to k-space and Fourier transformed to create a single A-line, representing the reflectance of light as a function of depth within tissue. Images comprising  $256 \times 701$  pixels over a dimension of 350 (longitudinal)  $\times$  501 (depth) mm were compiled by recording A-lines at each scan position. Axial resolution was 1.3 μm in tissue (estimated refractive index n=1.4) and the sensitivity was 90 dB. The lateral resolution was 4 μm over a depth of 300 μm. The working distance of the probe was approximately 200 μm. The high-resolution cross-sectional images recorded at 40 frames per second with this technology were critical for enabling the measurement of discrete hydration layers of the epithelium, as well as for the characterization of sub-cellular features.

Furthermore, the performance of this technology allowed dynamical events such as mucociliary transport and cilia beating to be captured.

Safety features incorporated into the clinical-grade system to ensure safe use of the device included a laser interlock switch, visible and audible indicators during active laser emission from the probe, and a laser power monitoring circuit. The optical power emission at the distal end of the probe was kept to 20 mW or less. Synchronization of operator and clinician controls, laser exposure, beam scanning, and data acquisition were achieved by way of a custom-built electronic control system. Apart from the intranasal probe and the attached handle unit, the entire optical system, electronic controller units, workstation and an articulating display screen were installed on a wheeled cart (Fig. 1C). Transportability and compactness ( $1.1 \times 0.6 \times 0.7$  m) of the clinical  $\mu$ OCT imaging system facilitated its use in a clinical setting, including a standard examination room.

### Image analysis

Manual maneuvering of the probe in unsedated subjects during image acquisition necessitated post-processing video stabilization prior to image analysis to extract measurements. Video stabilization was accomplished by cross-correlating successive frames to determine the lateral translation that was required to register the original images. Subsequently, methods similar to earlier published works were used to extract PCL, CBF, MCT, ASL, and ET (13, 49, fig. S6). The lateral extent of motile cilia coverage on epithelial surfaces was used to estimate pCC and automatic counting of globules was performed in ImageJ after segmentation of the globules. Further details on the image processing methods and a description of ex vivo sputum studies are given in the supplementary materials.

### Statistical analysis

Means were computed for each subject when at least three measures for each of the metrics were valid; mean values were used for subsequent cohort analysis. Data statistics are presented as mean (SD), unless indicated otherwise. Differences in each metric between CF and non-CF cohorts was compared cross-sectionally with either unpaired *t* test with Welch's correction or Mann-Whitney test, depending if the distribution of the measurements passed the Shapiro-Wilk normality test. Two-tailed *P* values are reported. Linear regression analysis and the Pearson correlation coefficient (*r*) were used to explore relationships between various metrics. Nonlinear quadratic regression analysis was used to analyze relation between ASL and MCT. Fisher's exact tests (for sex and race) and Mann-Whitney tests (for age) were performed to test for differences between proportions between CF and non-CF cohorts. One- and two-way ANOVA were used to measure differences in backscatter reflectance intensity or mucus viscosity, and Sildak's post hoc test was used to compare difference between groups if ANOVA was significant. Statistical analyses were performed using Prism 7.03 (Graphpad Software Inc.). Stepwise multivariate regression, power analysis, and intraclass correlation (ICC) (50, 51) was conducted using SAS 9.4 (SAS Institute Inc.); The original multivariate model included all variables with a linear relationship with MCT on univariate analysis (table S2, excluding ASL depth as this was non-linear and redundant to PCL). The criteria of *P*<0.05 was required during the stepwise

multivariate regression procedure to derive the most parsimonious models. A *P* value < 0.05 was considered statistically significant.

## Supplementary Material

Refer to Web version on PubMed Central for supplementary material.

## Acknowledgements:

We thank B. Battersby from Wellman Computational Core for helping to develop the data acquisition software. We thank C. Grant, S. Giddings, J. Gardecki, M. Rosenberg, G. Reeves and H. Hathorne for their help in this project. We thank Dr. L. Liu for his support.

**Funding:** We gratefully acknowledge the funding from NIH (5R01HL116213, R35HL135816, P30DK072482, and UL1TR001417) and Cystic Fibrosis Foundation (TEARNE16XX0, ROWE14Y0, and ROWE16XX0).

## References

1. Alexander BM, Petren EK, Rizvi S, Fink A, Ostrenga J, Sewall A, Loeffler D, Annual Data Report 2015. *Cyst. Fibros. Found. PatientRegist.*, 1–94 (2016).
2. Rowe SM, Miller S, Sorscher EJ, Cystic Fibrosis. *N. Engl. J. Med.* 352, 1992–2001 (2005). [PubMed: 15888700]
3. Ratjen F, Bell SC, Rowe SM, Goss CH, Quittner AL, Bush A, Cystic fibrosis. *Nat. Rev. Dis. Prim.* 1, 15010 (2015). [PubMed: 27189798]
4. Donaldson SH, Corcoran TE, Laube BL, Bennett WD, Mucociliary Clearance as an Outcome Measure for Cystic Fibrosis Clinical Research. *Proc. Am. Thorac. Soc.* 4, 399–405 (2007). [PubMed: 17652507]
5. McShane D, Davies JC, Wodehouse T, Bush A, Geddes D, Alton EWFW, Normal nasal mucociliary clearance in CF children: Evidence against a CFTR-related defect. *Eur. Respir. J.* 24, 95–100 (2004). [PubMed: 15293610]
6. Rowe SM, Accurso F, Clancy JP, Detection of Cystic Fibrosis Transmembrane Conductance Regulator Activity in Early-Phase Clinical Trials. *Proc. Am. Thorac. Soc.* 4, 387–398 (2007). [PubMed: 17652506]
7. Rowe SM, Heltshe SL, Gonska T, Donaldson SH, Borowitz D, Gelfond D, Sagel SD, Khan U, Mayer-Hamblett N, Van Dalsen JM, Joseloff E, Ramsey BW, Van Dalsen JM, Joseloff E, Ramsey BW, Clinical mechanism of the cystic fibrosis transmembrane conductance regulator potentiator ivacaftor in G551D-mediated cystic fibrosis. *Am. J. Respir. Crit. Care Med.* 190, 175–184 (2014). [PubMed: 24927234]
8. Chen J-H, Stoltz DA, Karp PH, Ernst SE, Pezzulo AA, Moninger TO, V Rector M, Reznikov LR, Launspach JL, Chaloner K, Zabner J, Welsh MJ, Loss of Anion Transport without Increased Sodium Absorption Characterizes Newborn Porcine Cystic Fibrosis Airway Epithelia. *Cell.* 143, 911–923 (2010). [PubMed: 21145458]
9. Welsh MJ, Rogers CS, Stoltz DA, Meyerholz DK, Prather RS, Development of a porcine model of cystic fibrosis. *Trans. Am. Clin. Climatol. Assoc.* 120, 149–162 (2009). [PubMed: 19768173]
10. Tarran R, Button B, Picher M, Paradiso AM, Ribeiro CM, Lazarowski ER, Zhang L, Collins PL, Pickles RJ, Fredberg JJ, Boucher RC, Normal and Cystic Fibrosis Airway Surface Liquid Homeostasis: The Effects of Phasic Shear Stress and Viral Infections. *J. Biol. Chem.* 280, 35751–35759 (2005). [PubMed: 16087672]
11. Button B, Cai L-H, Ehre C, Kesimer M, Hill DB, Sheehan JK, Boucher RC, Rubinstein M, A Periciliary Brush Promotes the Lung Health by Separating the Mucus Layer from Airway Epithelia. *Science.* 337, 937–41 (2012). [PubMed: 22923574]
12. Liu L, Gardecki JA, Nadkarni SK, Toussaint JD, Yagi Y, Bouma BE, Tearney GJ, Imaging the subcellular structure of human coronary atherosclerosis using micro-optical coherence tomography. *Nat. Med.* 17, 1010–1014 (2011). [PubMed: 21743452]

- Author Manuscript
- Author Manuscript
- Author Manuscript
- Author Manuscript
13. Oldenburg AL, Chhetri RK, Hill DB, Button B, Monitoring airway mucus flow and ciliary activity with optical coherence tomography. *Biomed. Opt. Express.* 3, 1978 (2012). [PubMed: 23024894]
  14. Lemieux BT, Chen JJ, Jing J, Chen Z, Wong BJF, Measurement of ciliary beat frequency using Doppler optical coherence tomography. *Int. Forum Allergy Rhinol.* 5, 1048–1054 (2015). [PubMed: 26136399]
  15. Jing JC, Chen JJ, Chou L, Wong BJFF, Chen Z, Visualization and Detection of Ciliary Beating Pattern and Frequency in the Upper Airway using Phase Resolved Doppler Optical Coherence Tomography. *Sci. Rep.* 7, 8522 (2017). [PubMed: 28819309]
  16. Zhou KC, Huang BK, Gamm UA, Bhandari V, Khokha MK, Choma MA, Particle streak velocimetry-optical coherence tomography: a novel method for multidimensional imaging of microscale fluid flows. *Biomed. Opt. Express.* 7, 1590 (2016). [PubMed: 27375926]
  17. Schulz-Hildebrandt H, Pieper M, Stehmar C, Ahrens M, Idel C, Wollenberg B, König P, Hüttmann G, Novel endoscope with increased depth of field for imaging human nasal tissue by microscopic optical coherence tomography. *Biomed. Opt. Express.* 9, 636 (2018). [PubMed: 29552400]
  18. Birket SE, Chu KK, Liu L, Houser GH, Diephuis BJ, Wilsterman EJ, Dierksen G, Mazur M, Shastry S, Li Y, Watson JD, Smith AT, Schuster BS, Hanes J, Grizzle WE, Sorscher EJ, Tearney GJ, Rowe SM, A functional anatomic defect of the cystic fibrosis airway. *Am. J. Respir. Crit. Care Med.* 190, 421–432 (2014). [PubMed: 25029666]
  19. Tuggle KL et al., Characterization of defects in ion transport and tissue development in Cystic Fibrosis Transmembrane Conductance Regulator (CFTR)-knockout rats. *PLoS One.* 9, 1–14 (2014).
  20. Birket SE, Chu KK, Houser GH, Liu L, Fernandez CM, Solomon GM, Lin V, Shastry S, Mazur M, Sloane P, Hanes J, Grizzle WE, Sorscher EJ, Tearney GJ, Rowe SM, Combination Therapy with Cystic Fibrosis Transmembrane Conductance Regulator Modulators Augment the Airway Functional Microanatomy. *Am. J. Physiol. - Lung Cell. Mol. Physiol* 310, L928–L939 (2016). [PubMed: 26968770]
  21. Rowe SM, Clancy JP, Wilschanski M, in *Cystic Fibrosis. Methods in Molecular Biology (Methods and Protocols)*, Amaral M KK, Ed. (Humana Press, 2011; <http://link.springer.com/10.1007/978-1-61779-120-8>), vol. 742.
  22. Berkhouit MC, Van Rooden CJ, Rijntjes E, Fokkens WJ, El Bouazzaoui LH, Heijerman HGM, Sinonasal manifestations of cystic fibrosis: A correlation between genotype and phenotype? *J. Cyst. Fibros.* 13, 442–448 (2014). [PubMed: 24210900]
  23. Chu KK, Unglert C, Ford TN, Cui D, Carruth RW, Singh K, Liu L, Birket SE, Solomon GM, Rowe SM, others, In vivo imaging of airway cilia and mucus clearance with micro-optical coherence tomography. *Biomed. Opt. Express.* 7, 2494–2505 (2016). [PubMed: 27446685]
  24. Cui D, Chu KK, Yin B, Ford TN, Hyun C, Leung HM, Gardecki JA, Solomon GM, Birket SE, Liu L, others, Flexible, high-resolution micro-optical coherence tomography endobronchial probe toward in vivo imaging of cilia. *Opt. Lett.* 42, 867–870 (2017). [PubMed: 28198885]
  25. Hamutcu R, Rowland JM, V Horn M, Kaminsky C, MacLaughlin EF, Starnes VA, Woo MS, Clinical Findings and Lung Pathology in Children with Cystic Fibrosis. 165, 1172–1175 (2002).
  26. Rogers CS et al., Disruption of the CFTR Gene Produces a Model of Cystic Fibrosis in Newborn Pigs. *Science.* 321, 1837–1841 (2008). [PubMed: 18818360]
  27. Birket SE, Davis JM, Fernandez CM, Tuggle KL, Oden AM, Chu KK, Tearney GJ, Fanucchi MV, Sorscher EJ, Rowe SM, Development of an airway mucus defect in the cystic fibrosis rat. *JCI Insight.* 3, 1–14 (2018).
  28. Chu KK, Kusek ME, Liu L, Som A, Yonker LM, Leung HM, Cui D, Ryu J, Eaton AD, Tearney GJ, Hurley BP, Illuminating dynamic neutrophil transepithelial migration with micro-optical coherence tomography. *Sci. Rep.* 8, 45789 (2017). [PubMed: 28368012]
  29. Henderson G, Ehre C, Button B, Abdullah LH, Cai LH, Leigh MW, DeMaria GC, Matsui H, Donaldson SH, Davis CW, Sheehan JK, Boucher RC, Kesimer M, Cystic fibrosis airway secretions exhibit mucin hyperconcentration and increased osmotic pressure. *J. Clin. Invest.* 124, 3047–3060 (2014). [PubMed: 24892808]
  30. Liu L, Shastry S, Byan-Parker S, Houser G, Chu KK, Birket SE, Fernandez CM, Gardecki JA, Grizzle WE, Wilsterman EJ, Sorscher EJ, Rowe SM, Tearney GJ, An autoregulatory mechanism

- governing mucociliary transport is sensitive to mucus load. *Am. J. Respir. Cell Mol. Biol.* 51, 485–493 (2014).
31. Ostedgaard LS, Moninger TO, McMenimen JD, Sawin NM, Parker CP, Thornell IM, Powers LS, Gansemer ND, Bouzek DC, Cook DP, Meyerholz DK, Abou Alaiwa MH, Stoltz DA, Welsh MJ, Gel-forming mucins form distinct morphologic structures in airways. *Proc. Natl. Acad. Sci.* 114, 201703228 (2017).
  32. Yuan S, Hollinger M, Lachowicz-Scroggins ME, Kerr SC, Duncan EM, Daniel BM, Ghosh S, Erzurum SC, Willard B, Hazen SL, Huang X, Carrington SD, Oscarson S, Fahy JV, Oxidation increases mucin polymer cross-links to stiffen airway mucus gels. *Sci. Transl. Med.* 7, 1–10 (2015).
  33. Quinton PM, Cystic fibrosis: impaired bicarbonate secretion and mucoviscidosis. *Lancet.* 372, 415–417 (2008). [PubMed: 18675692]
  34. Ridley C, Kirkham S, Williamson SJ, Davis CW, Woodman P, Thornton DJ, Biosynthesis of the polymeric gel-forming mucin MUC5B. *Am. J. Physiol. Cell. Mol. Physiol.* 310, L993–L1002 (2016).
  35. Gustafsson JK, Ermund A, Ambort D, V Johansson MEV, Nilsson HE, Thorell K, Hebert H, Sjövall H, Hansson GC, Bicarbonate and functional CFTR channel are required for proper mucin secretion and link cystic fibrosis with its mucus phenotype. *J. Exp. Med.* 209, 1263–1272 (2012). [PubMed: 22711878]
  36. Hoegger MJ, Fischer AJ, McMenimen JD, Ostedgaard LS, Tucker AJ, Awadalla MA, Moninger TO, Michalski AS, Hoffman EA, Zabner J, Stoltz DA, Welsh MJ, Impaired mucus detachment disrupts mucociliary transport in a piglet model of cystic fibrosis. *Science.* 345, 818–822 (2014). [PubMed: 25124441]
  37. Matsui H, Grubb BR, Tarhan R, Randell SH, Gatzky JT, Davis CW, Boucher RC, Evidence for periciliary liquid layer depletion, not abnormal ion composition, in the pathogenesis of cystic fibrosis airways disease. *Cell.* 95, 1005–1015 (1998). [PubMed: 9875854]
  38. Garcia MAS, Yang N, Quinton PM, Normal mouse intestinal mucus release requires cystic fibrosis transmembrane regulator-dependent bicarbonate secretion. *J. Clin. Invest.* 119, 2613–2622 (2009). [PubMed: 19726884]
  39. Thornton DJ, From Mucins to Mucus: Toward a More Coherent Understanding of This Essential Barrier. *Proc. Am. Thorac. Soc.* 1, 54–61 (2004). [PubMed: 16113413]
  40. Sahin-Yilmaz A, Naclerio RM, Anatomy and physiology of the upper airway. *Proc. Am. Thorac. Soc.* 8, 31–39 (2011). [PubMed: 21364219]
  41. Oltmanns U, Palmowski K, Wielputz M, Kahn N, Baroke E, Eberhardt R, Wege S, Wiebel M, Kreuter M, Herth FJF, Mall MA, Optical coherence tomography detects structural abnormalities of the nasal mucosa in patients with cystic fibrosis. *J. Cyst. Fibros.* 15, 216–222 (2016). [PubMed: 26211604]
  42. Mahmood U, Ridgway J, Jackson R, Guo S, Su J, Armstrong W, Shibuya T, Crumley R, Chen Z, Wong B, In vivo optical coherence tomography of the nasal mucosa. *Am. J. Rhinol.* 20, 155–159 (2006). [PubMed: 16686378]
  43. Henke MO, Ratjen F, Mucolytics in cystic fibrosis. *Paediatr. Respir. Rev.* 8, 24–29 (2007). [PubMed: 17419975]
  44. Kolaczkowska E, Kubes P, Neutrophil recruitment and function in health and inflammation. *Nat. Rev. Immunol.* 13, 159–175 (2013). [PubMed: 23435331]
  45. Niemiec MJ, De Samber B, Garrevoet J, Vergucht E, Vekemans B, De Rycke R, Björn E, Sandblad L, Wellenreuther G, Falkenberg G, Cloetens P, Vincze L, Urban CF, Trace element landscape of resting and activated human neutrophils on the submicrometer level. *Metalomics.* 7, 996–1010 (2015). [PubMed: 25832493]
  46. Bamberg R, Johnson J, Segmented neutrophil size and platelet morphology in HIV/AIDS patients. *Clin Lab Sci.* 15, 18–22 (2002). [PubMed: 12778952]
  47. Van Lommel ATL, From cells to organs: a histology textbook and atlas (Springer Science & Business Media, 2003).
  48. Hyun C, Leung HM, Ford TN, Birket SE, Solomon GM, Woodworth BA, Cho D-Y, Rowe SM, Guillermo GT, in SPIE BiOEndoscopic Microscopy XIII (San Francisco, USA, 2018).

49. Liu L, Chu KK, Houser GH, Diephuis BJ, Li Y, Wilsterman EJ, Shastry S, Dierksen G, Birket SE, Mazur M, others, Method for quantitative study of airway functional microanatomy using micro-optical coherence tomography. *PLoS One*. 8, e54473 (2013).
50. McGraw KO, Wong SP, Forming Inferences About Some Intraclass Correlation Coefficients. *Psychol. Methods*. 1, 30–46 (1996).
51. Koo TK, Li MY, A Guideline of Selecting and Reporting Intraclass Correlation Coefficients for Reliability Research. *J. Chiropr. Med.* 15, 155–163 (2016). [PubMed: 27330520]
52. Teo JC, Foin N, Otsuka F, Bulluck H, Fam JM, Wong P, Low FH, Leo HL, Mari JM, Joner M, Girard MJA, Virmani R, Optimization of coronary optical coherence tomography imaging using the attenuation-compensated technique: A validation study. *Eur. Heart J. Cardiovasc. Imaging*. 18, 880–887 (2017). [PubMed: 27469587]
53. Eliceiri K, Schneider CA, Rasband WS, Eliceiri KW, NIH Image to ImageJ : 25 years of image analysis. *Nat. Methods*. 9, 671–675 (2012). [PubMed: 22930834]
54. Labno C, Two Ways to Count Cells with ImageJ, 1–5 (2014).
55. Soille P, Vincent LM, Determining watersheds in digital pictures via flooding simulations. *Proc. SPIE*. 1360, 240–250 (1990).
56. Tearney GJ, Brezinski ME, Southern JF, Bouma BE, Hee MR, Fujimoto JG, Determination of the refractive index of highly scattering human tissue by optical coherence tomography. *Opt. Lett.* 20, 2258 (1995). [PubMed: 19862316]

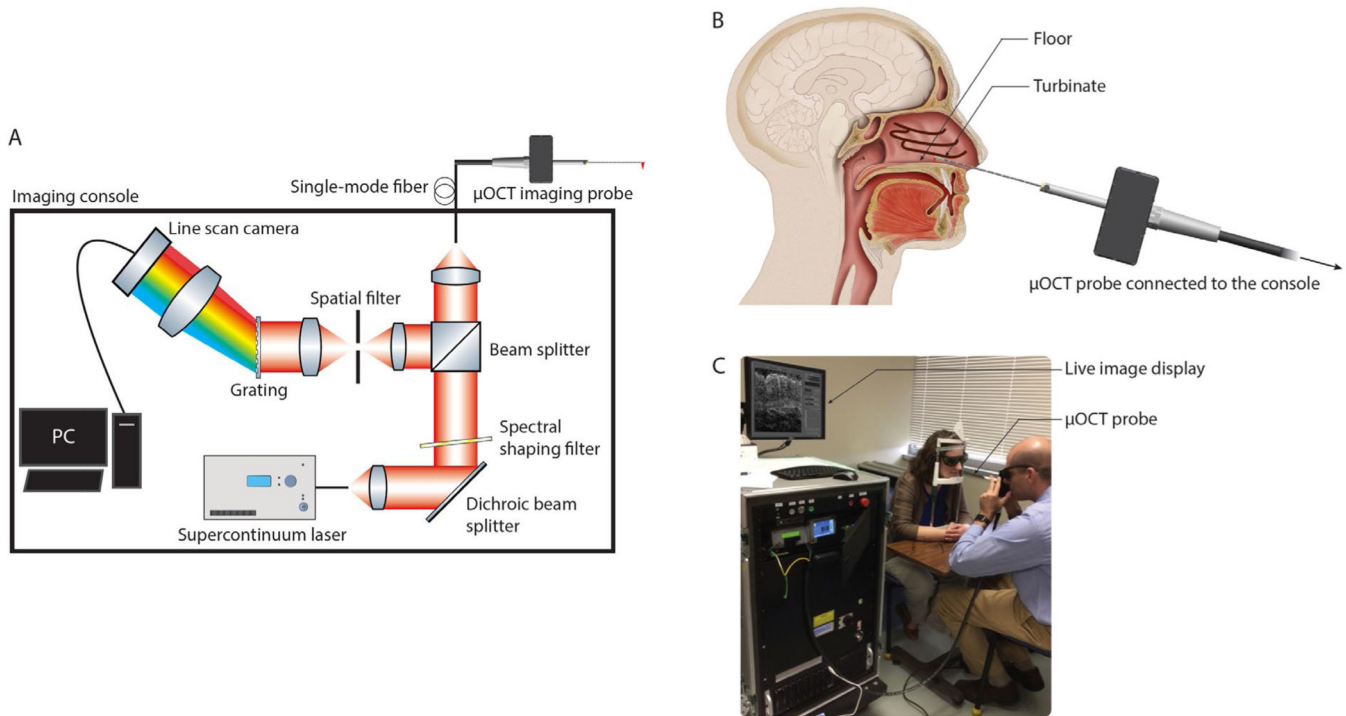


**Fig. 1. Schematic of the μOCT imaging system, illustration of the clinical device, and its use in human subjects.**

(A) Broadband light from a supercontinuum laser was first filtered to achieve a Gaussian-like spectral shape, before a portion of the light was directed into the side-viewing μOCT catheter. Through linear motion transduced by a piezoelectric motor, the beam was scanned longitudinally over a distance of 350  $\mu\text{m}$  at a rate of 40 Hz. Light returning from the tissue was relayed to a spectrometer constructed from a 940 lines/mm volume phase holographic grating, a camera lens, and a CMOS line scan camera. The spectrometer detected a full-width-half-maximum spectral range of  $800 \pm 150 \text{ nm}$  and 2500-pixel spectrograms were recorded at a rate of 20 kHz during data acquisition. (B) Schematic showing how the clinician positioned the imaging catheter under live imaging guidance and recorded data from various positions in the turbinate and floor regions in the nasal inferior meatus. (C) Photograph of a demonstration of the clinical procedure.

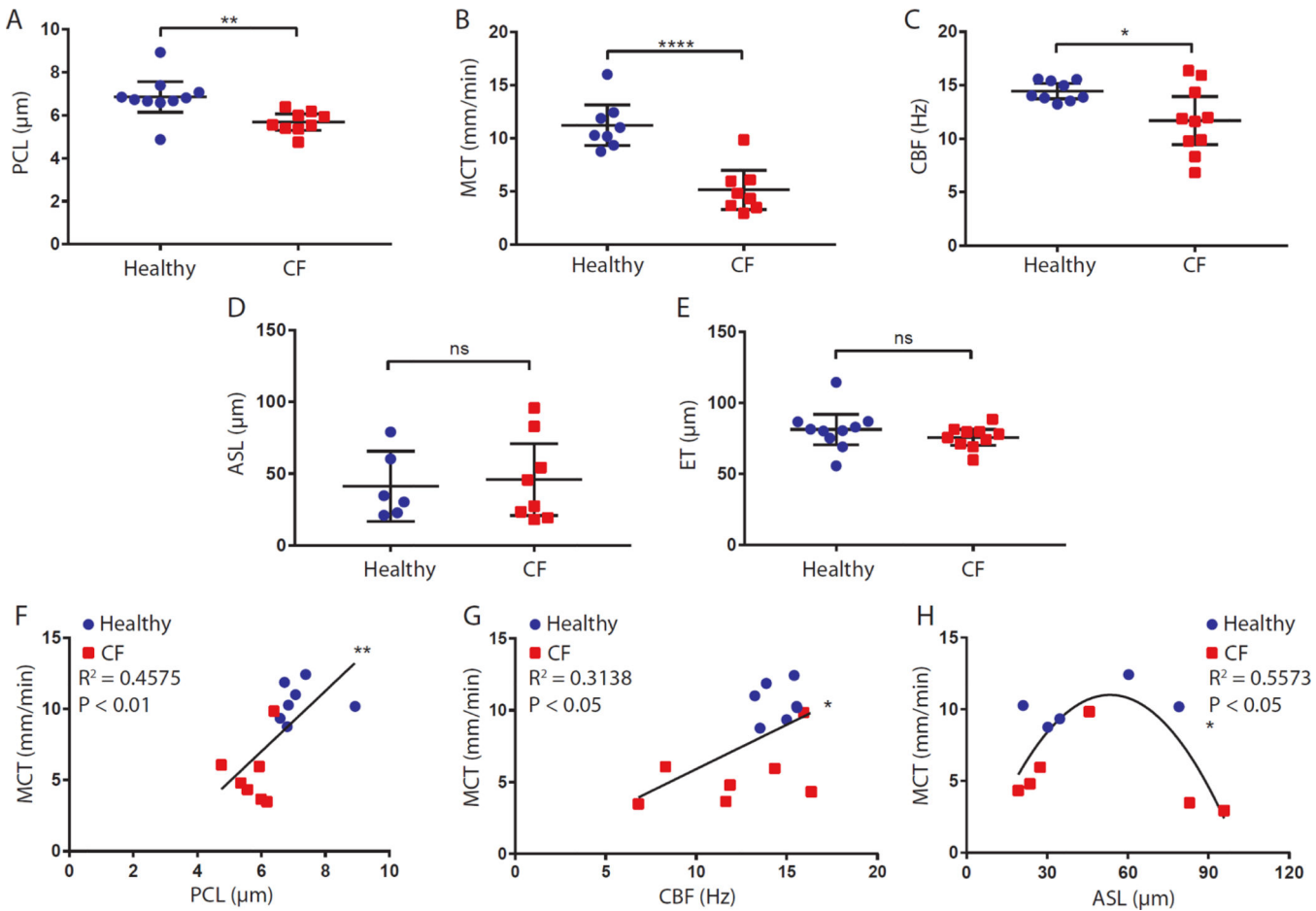


**Fig. 2. Functional microanatomy measurements from  $\mu\text{OCT}$  images.**

(A to E) Scatter plots of PCL, MCT, CBF, ASL, and ET measurements of healthy and CF cohorts. (F and G) Scatter plots with linear fits of PCL (F) and CBF (G) versus MCT. Only subjects with PCL, MCT, and CBF that were all successfully measured ( $n = 14$ ) were included in the analysis. (H) Scatter plots with nonlinear fit of ASL versus MCT ( $n = 11$ ) showing a quadratic relation. Each data point represents the mean measurement for each individual. Bars are means and 95% CI. Comparison of data in (A) by Mann-Whitney test, and (B to E) by  $t$  test with Welch's correction. All linear and nonlinear fits in (F) to (H) were performed with the combined data from both CF (red) and non-CF (blue) cohorts. \* $P < 0.05$ ; \*\* $P < 0.01$ ; \*\*\* $P < 0.0001$ . PCL: Periciliary liquid layer depth; MCT: Mucociliary transport rate; CBF: Ciliary beat frequency; ASL: Airway surface liquid layer depth; ET: Epithelium thickness.

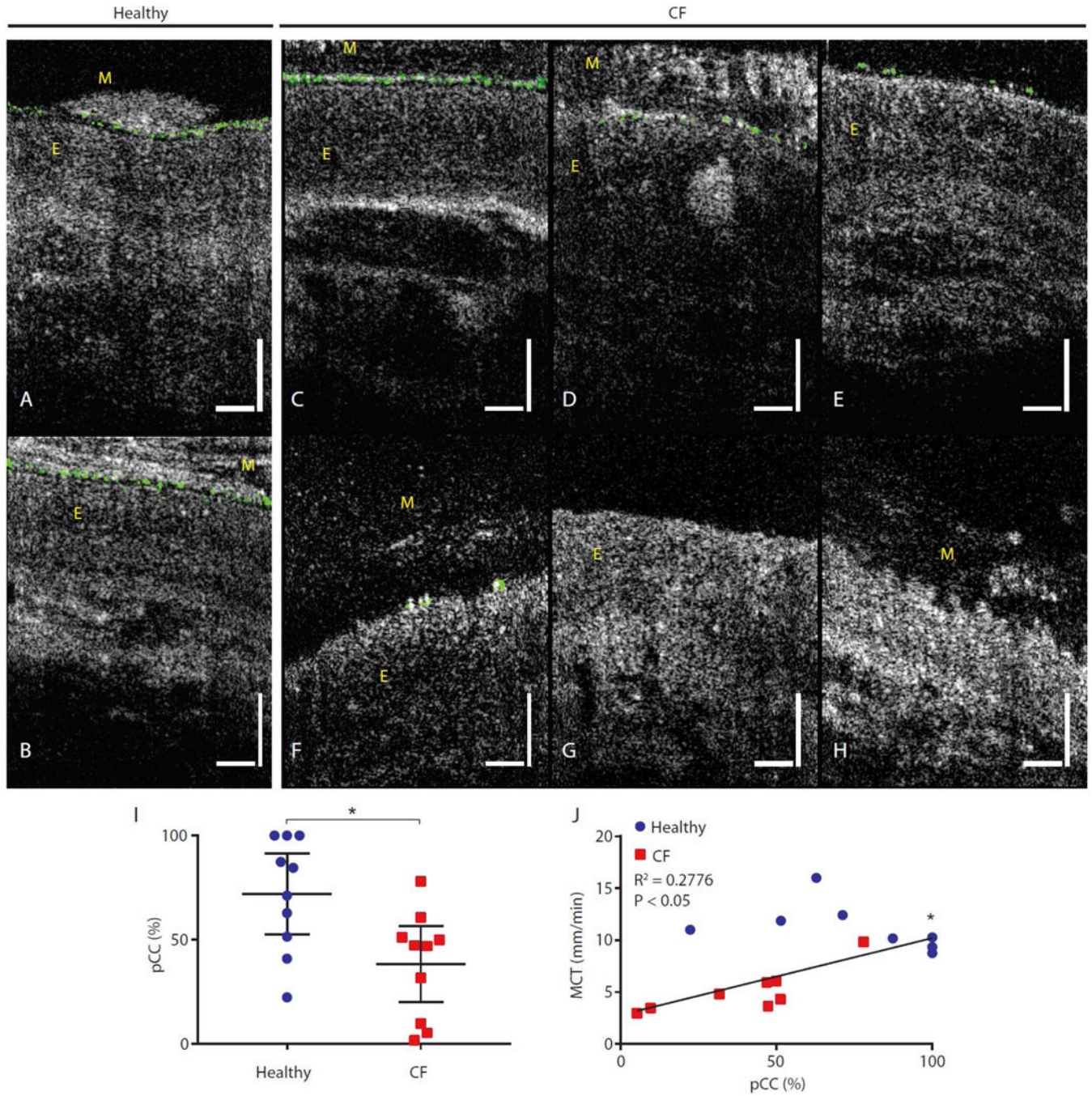


**Fig. 3. Representative images of disruption of the PCL in CF subjects compared to healthy non-CF controls.**

(A and B) PCL images from healthy subjects. Uniform and contiguous PCL (dark band beneath the layer of cilia) was seen preventing mucus load from coming in direct contact with the epithelium. (C to H) Intact PCL (C) was sometimes observed in CF patients, but diminished and discontinuous PCL (D and E) was prevalent. An instance where epithelium was sparsely ciliated was observed (F), resulting in a complete absence of PCL despite the presence of cilia. (G) An instance in which the epithelium was completely devoid of cilia.

(H) Denuded epithelium with a characteristically rough surface. Vertical and horizontal bars = 50  $\mu$ m. Motile cilia are pseudo-colored in green for easy visualization. Mucus and epithelium are indicated with M and E, respectively. (I) Scatter plot of pCC measurements of healthy and CF cohorts. (J) Scatter plot with linear fit of pCC and MCT ( $n = 16$ ). Each data point represents the mean measurement for each individual. Bars are means and 95% CI. Comparison of data in (I) by  $t$  test with Welch's correction. Linear fit in (J) was performed with the combined data from both CF (red) and non-CF (blue) cohorts. \* $P < 0.05$ ; MCT: Mucociliary transport rate; pCC: Percent cilia coverage.

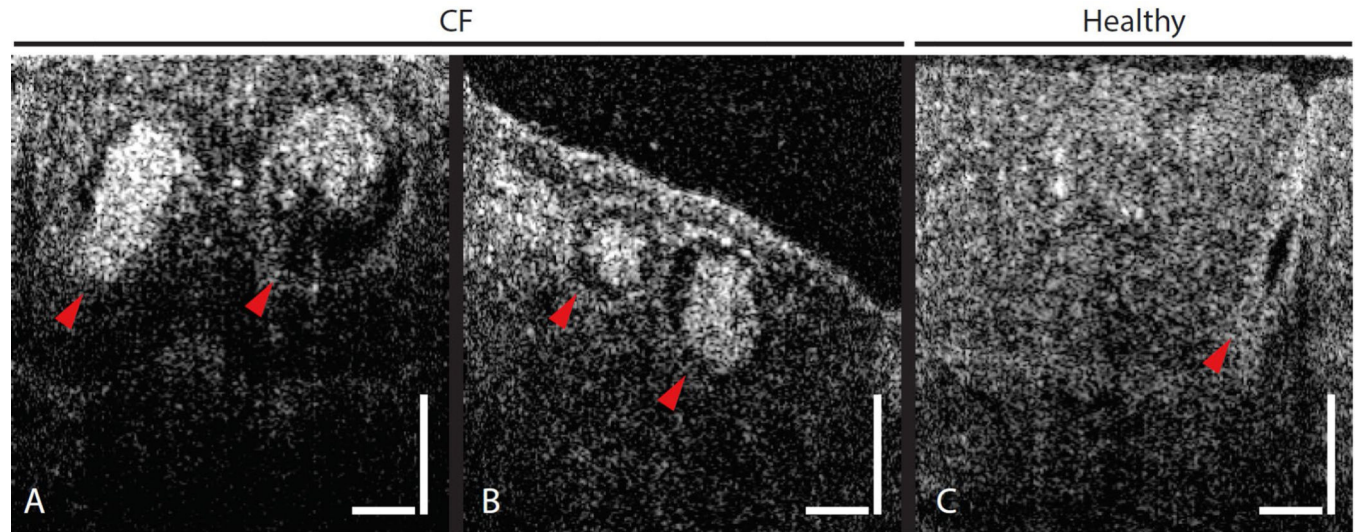


**Fig. 4. Comparison between healthy and CF gland ducts.**

(A and B) Large round features just beneath the epithelial surfaces were seen in  $\mu$ OCT images of mucosa of a few subjects with CF. (C) A  $\mu$ OCT image of a healthy gland duct. Arrowheads point to gland ducts. Vertical and horizontal bars = 50  $\mu$ m.

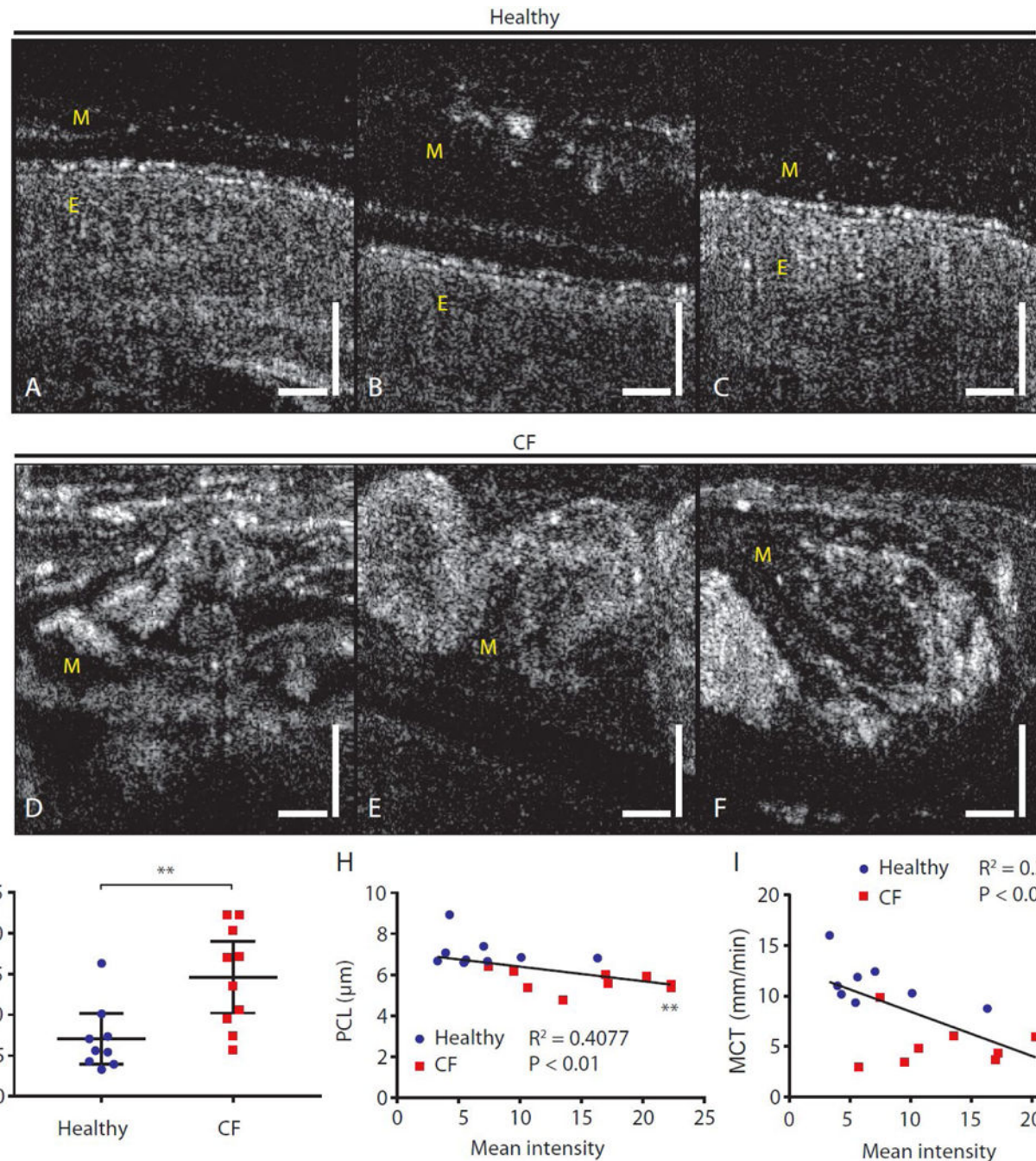


**Fig. 5. Prominent and heterogeneous mucus reflectance intensity in CF subjects as compared to healthy non-CF controls.**

(A to C) Typical  $\mu$ OCT images from healthy subjects showing continuous PCL, smooth epithelial surfaces, and a weakly scattering mucus layer above the ciliary layer. (D to F) Images from CF subjects showing highly reflective and heterogeneous mucus with distinctive structure accumulated to large thicknesses. View of the underlying epithelial tissue is obscured by mucus. (G) Scatter plot showing mean mucus reflectance intensity in CF compared to healthy non-CF controls. (H and I) Correlations between mean mucus

reflectance intensity in vivo and airway hydration reflected by PCL depth (H) and MCT rate (I). Vertical and horizontal bars = 50  $\mu\text{m}$ . \* $P<0.05$ ; \*\* $P<0.01$  by Mann-Whitney test. PCL: Periciliary liquid layer depth; MCT: Mucociliary transport rate. Mucus and epithelium are indicated with M and E, respectively.

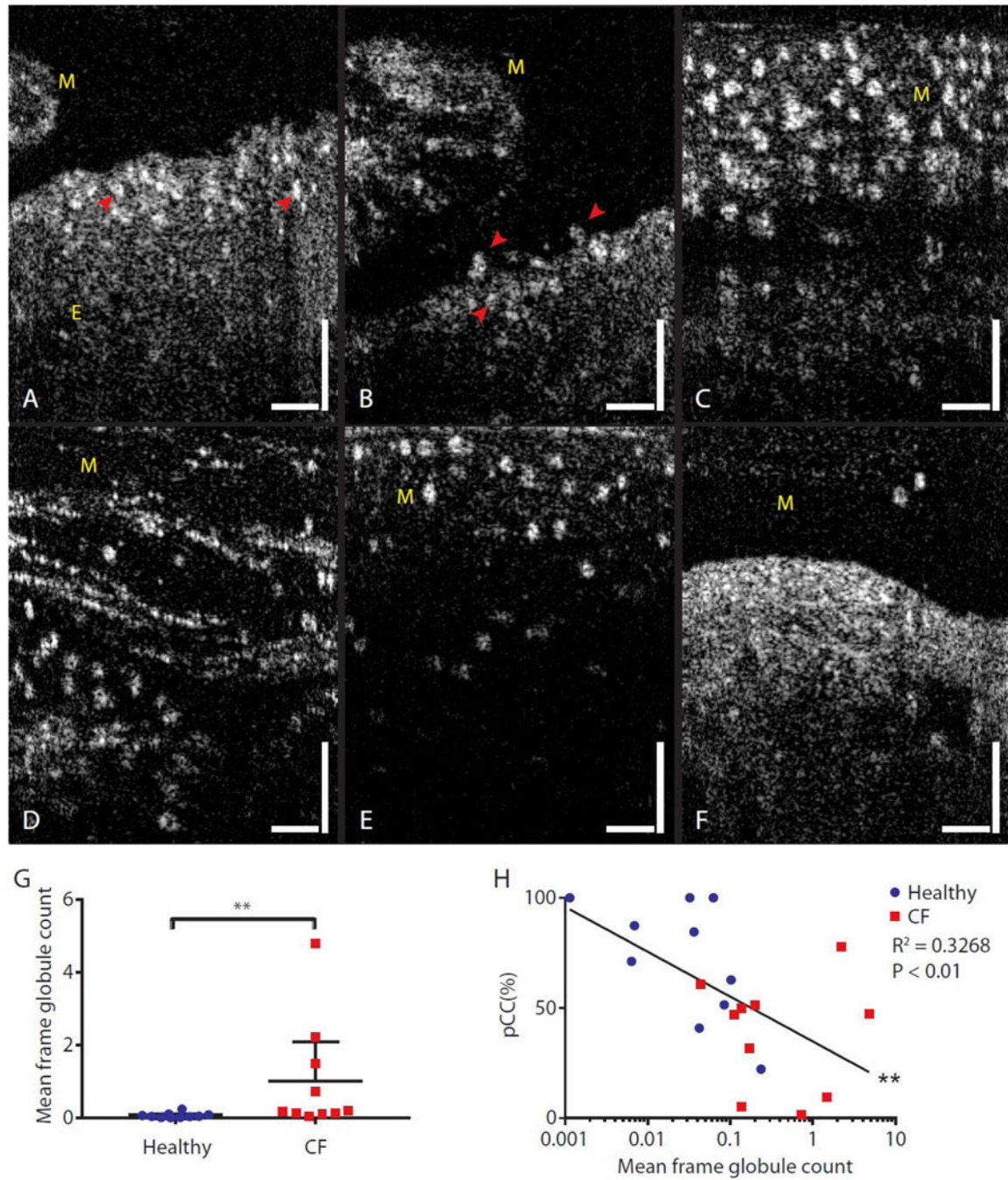


**Fig. 6. Prevalence of spherical granulocyte-appearing globules in CF airways suggesting inflammatory cell infiltration.**

(A to F)  $\mu$ OCT images of globular structures near the top of the epithelium (A and B, indicated with arrowheads), above the epithelium (B, indicated with arrowheads), and embedded in secreted mucus (C to F). Vertical and horizontal bars = 50  $\mu$ m. (G) A scatter plot of mean frame globule count in mucus of healthy non-CF subjects and subjects with CF. Bars are mean and 95% CI. \*\* $P < 0.01$  by Mann-Whitney test. (H) Correlation of pCC plotted against mean frame globule count for each subject, color coded by disease state.

Semi-log correlation had  $R^2$  of 0.3268, \*\* $P<0.01$ . pCC: Percent cilia coverage. Mucus and epithelium are indicated with M and E, respectively.

Author Manuscript

Author Manuscript

Author Manuscript

Author Manuscript

**Table 1.**  
**Summary of key MCC measures.**

ICC: Intraclass correlation. PCL: Periciliary liquid layer depth; MCT: Mucociliary transport rate; CBF: Ciliary beat frequency; ASL: Airway surface liquid layer depth; ET: Epithelium thickness; pCC: Percent cilia coverage.

Metric	non-CF		CF		P-value	Measure- ment success rate (%)	ICC for intra- observer reliability	ICC for inter- observer reliability
	mean	95% CI	mean	95% CI				
PCL ( $\mu\text{m}$ )	6.9	6.1–7.6	5.6	5.2–6.0	<0.01	95	0.9866	0.8844
MCT (mm/min)	11.2	9.3–13.1	5.1	3.3–7.0	<0.0001	80	0.9994	0.9895
CBF (Hz)	14.4	13.7–15.2	11.7	9.4–13.9	<0.05	95	0.9752	0.9505
ASL ( $\mu\text{m}$ )	41.4	17.0–65.8	45.9	20.9–70.9	0.7537	70	0.9977	0.9982
ET ( $\mu\text{m}$ )	81.3	70.6–92.0	75.4	69.8–81.0	0.3127	100	0.9972	0.9927
pCC (%)	72.1	52.5–91.6	38.2	20.0–56.5	<0.05	100	0.9998	0.9985